



## **Using photogrammetry-based imperfection measurement tools to determine the impact of corner radii imperfection on cold-formed steel member strength**

Abbas Joorabchian<sup>1</sup>, Kara D. Peterman<sup>2</sup>

### **Abstract**

Despite recent advances in imperfection measurement tools, accurate corner radius measurements have remained elusive. While imperfect corner radii can impact section properties. The objectives of this research project are to (i) quantify the impact of imperfect corner radii on cold-formed steel member strength, (ii) provide a tool to determine cross-section imperfections via photogrammetry-based image processing. Lipped channel sections with imperfect corner radii are analyzed using the finite strip method and their stability characteristics are compared to those of the corresponding perfect sections. Analyses presented herein demonstrate that any increase in corner radii can have an impact on the strength of the sections. Additionally, the work examines the role of section geometry and aspect ratio in the observed differences. Various sections are studied to examine the impacts of web-flange aspect ratio and proportion comprised of corner radius. The second component of the work introduces a low-cost, open access, and easily-distributed imperfection measurement tool utilizing photogrammetry. With this new tool, users are able to capture accurate cross-section measurements (including corner radius) with a standard cell phone camera and directly input the measurements into finite strip method analysis. Several examples are done in a lab by a cell phone camera and nominal dimension of sections are compared to their accurate one.

### **1. Introduction**

Cold-formed steel (CFS) members are widely used due to their high strength to weight ratio, cost-effectiveness, recyclability, reduced shipping costs, weather resistance, and non-combustibility. CFS members are not perfect and their dimensions and material properties are different from nominal properties. There are several types of imperfection: geometric, material strength, residual stress, loading, and support conditions (Dubina & Ungureanu, 2002). Manufacturing processes, shipping, storage, and construction can all cause geometric imperfections CFS members have thin walls (from 0.03 inches to 0.1 inches) which makes the result of computational analysis and the behavior of structures imperfection sensitive (Zeinoddini-Meimand, 2011). Cold bending of the steel sheets (which makes round corners into the section) leaves complex residual stresses and strains (Moen, Igusa, & Schafer, 2008), (Zeinoddini & Schafer, 2010). Research has been conducted to determine the impact of section imperfection on the strength of CFS members and

---

<sup>1</sup> PhD Candidate, University of Massachusetts Amherst, <ajoorabchian@umass.edu>

<sup>2</sup> Assistant Professor, University of Massachusetts Amherst, <kdpeterman@umass.edu>

imperfection measurement tools; the literature and existing researches herein are summarized below, while corner radius measurement requires more researches because of the impact of imperfect corner radii on the section properties. This research project quantifies the impact of imperfect corner radii on cold-formed steel member strength.

In order to explore the impact of imperfections, first, they should be measured. Schafer and Peköz (1998) collected statistical results for geometric imperfections. Their method considered two types of imperfection: local web ( $d_1$ ) and local flange ( $d_2$ ), as shown in Figure 1. Schafer and Peköz (1998) utilized a milling machine and a direct current different transformer (DCDT). In other words, this method used contact instrument and the data focused only on maximum imperfections. The limitations in contact imperfection measurements motivated scholars to employ advanced technologies such as sensor and laser and propose non-contact measurement tools. Young and Rasmussen (2003) built a system utilizing five linear voltage displacement transducers (LVDTs) and a stepper motor to move the measurement frames along the desired specimen for measuring for measuring both web and flange imperfections. McAnallen et al. (2014) provided two photogrammetry-based and laser triangulation techniques to take 3D measurements. A laser-based imperfection measurement platform was designed and configured by Zhao, Tootkaboni, and Schafer (2017). This platform uses an accurate line laser scanner for measuring sections dimensions. This platform consists of a rotary ring and a linear motion system to enable the laser to rotate and move along the desired specimen.

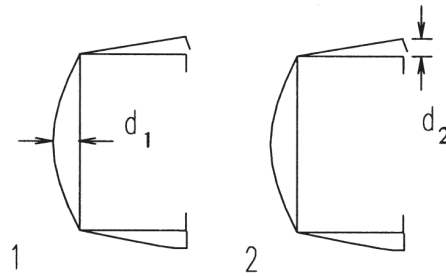


Figure 1: Definition of geometric imperfection (Schafer & Peköz, 1998)

A large variety of different systems have been utilized to measure the section imperfections. However, as shown in Figure 2, for instance, laser-based imperfection measurement platform utilizes expensive equipment such as laser scanner which is not affordable or portable. The tool provided herein in this research project gives all users including scholars and engineers in construction sites this possibility to measure geometric imperfections of sections just by simple images taken by a standard cell phone camera. This tool can be utilized as a corner measurement tool in labs. This paper starts with exploring the impact of corner radius imperfection on the CFS strength and then a brief explanation about the methodology of the tool especially in measuring the corner radius. The procedure of measuring the corner radius and examples follow.

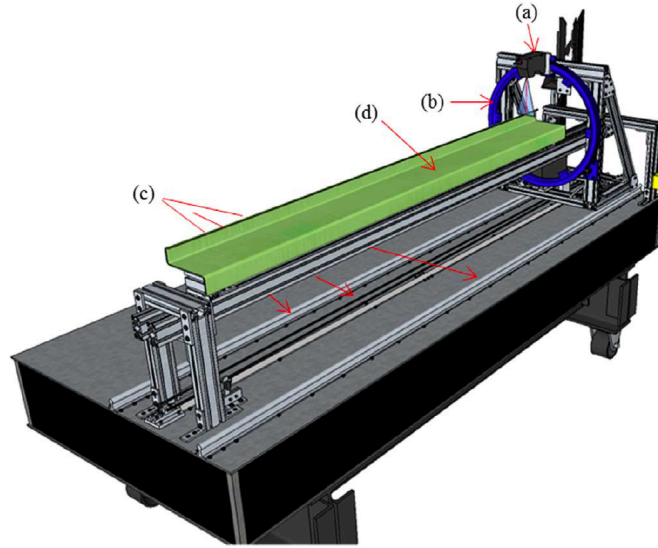


Figure 2: Imperfection measurement platform used by Zhao, Tootkaboni, and Schafer (2017); (a) laser scanner; (b) rotary stage; (c) linear motion system; (d) specimen

## 2. Corner radius imperfection

Corner radius imperfections refer to the condition in which a section has a corner radius greater or smaller than its nominal one. Every CFS member consists of two parts: flat plates and round corners. The increase of corner radius decreases the length of flat parts, along with the decrease in section area. They can impact the strength of CFS sections and should be considered in design methods (Zeinoddini & Schafer, 2010). Several factors can influence the amount of corner radius impact such as  $r/t$  ratio. In order to examine the role of only web to flange ratio in the observed differences, four CFS lipped channels are selected with same  $r/t$  ratio. In other words, the goal of this section is probing the role of web length to flange length ratio in addition to the contribution of corner area in section area. The selected sections are 250S162-68, 362S162-68, 600S300-68, and 1000S350-68. The geometry of these sections is shown in Table 1.

Table 1: Geometry information of sections analyzed herein

Section	Member depth (in.) *	Flange width (in.) *	Corner radius (in.) *	Stiffening lip length (in.) *	Thickness (in.)
250S162-68	2.432	1.552	0.1409	0.466	0.068
362S162-68	3.552	1.552	0.1409	0.466	0.068
600S300-68	5.932	2.932	0.1409	0.591	0.068
1000S350-68	9.932	3.432	0.1409	0.966	0.068

\*Dimensions are center to center

To explore the impact of corner radii on stability performances, the corner radii of the nominal sections are increased parametrically in CUFSM (Schafer & Ádány, 2006). Pinned-pinned boundary conditions are defined for the sections and one concentrated load is applied on top of each column (Table 2). Finite strip method analysis is performed for each section and the local and distortional buckling loads are calculated and compared. The signature curves of perfect sections are plotted in Figure 3. It should be noted that all of the sections cannot be increased by same

percentage. For instance, corner radius of 250S162-68 cannot be increased 400 percent due to the fact that in this case, the section no longer has a flat lip.

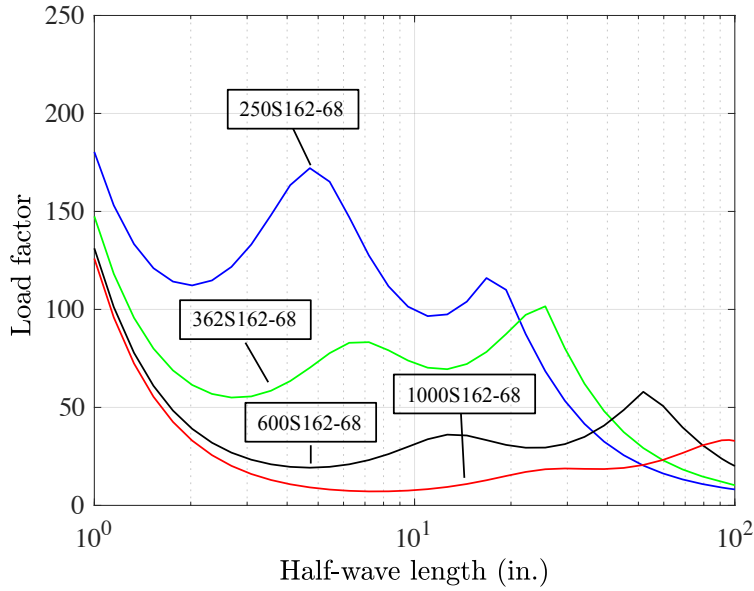


Figure 3: Signature curves of perfect sections

Table 2: Local buckling load of nominal and imperfect sections

Section	Percentage radius increased (%)	New corner radius (in.)	Section area (A) (in. <sup>2</sup> )	Corner area (Ar) (in. <sup>2</sup> )	A <sub>r</sub> /A (%)	Local buckling load (kips)	Distortional buckling load (kips)	Difference in local buckling (%)	Difference in distortional buckling load (%)
250S162-68	0	0.14	0.42	0.06	14.23	47.47	40.85	-	-
	50	0.19	0.42	0.08	19.93	48.61	40.38	2.40	-1.15
	100	0.25	0.41	0.11	25.81	50.89	39.92	7.19	-2.30
	200	0.35	0.40	0.15	38.14	59.13	39.26	24.54	-3.91
	300	0.46	0.39	0.20	51.27	71.00	39.46	49.55	-3.41
362S162-68	0	0.14	0.50	0.06	12.06	27.47	34.69	-	-
	50	0.19	0.49	0.08	16.85	27.74	34.29	1.00	-1.15
	100	0.25	0.49	0.11	21.77	28.32	33.94	3.11	-2.17
	200	0.35	0.47	0.15	32.00	30.45	33.23	10.87	-4.22
	300	0.46	0.46	0.20	42.80	33.76	33.26	22.91	-4.11
600S300-68	0	0.14	0.87	0.06	6.95	16.65	25.48	-	-
	50	0.19	0.86	0.08	9.66	16.69	25.34	0.25	-0.53
	100	0.25	0.85	0.11	12.41	16.82	25.20	1.02	-1.10
	200	0.35	0.84	0.15	18.04	17.41	24.93	4.60	-2.16
	300	0.46	0.83	0.20	23.84	18.50	24.78	11.13	-2.73
	400	0.57	0.82	0.24	29.82	20.00	24.89	20.15	-2.32
1000S350-68	0	0.14	1.26	0.06	4.79	8.96	23.30	-	-
	50	0.19	1.25	0.08	6.64	8.96	23.15	0.00	-0.65
	100	0.25	1.24	0.11	8.51	8.97	22.99	0.13	-1.32
	200	0.35	1.23	0.15	12.31	9.06	22.68	1.16	-2.67
	300	0.46	1.22	0.20	16.19	9.26	22.38	3.37	-3.98
	400	0.57	1.21	0.24	20.15	9.57	22.08	6.77	-5.23
	500	0.68	1.19	0.29	24.19	9.95	22.10	11.09	-5.16
	600	0.79	1.18	0.33	28.32	10.39	21.99	16.00	-5.65
700	0.89	1.17	0.38	32.55	10.87	22.01	21.27	-5.54	

As shown in Table 2 and Figure 4, imperfect sections have greater local buckling load in compared to those of the corresponding perfect sections due to the fact that in the local buckling the orthogonality between web and flange corner is not maintained. As a result, an increased corner radius increases the section strength against local buckling. Table 2 and Figure 5 illustrate imperfect sections have less distortional buckling loads. The corner radius imperfection has less impact on the strength of specimens which have larger webs and flanges. In fact, this less impact is related to the contribution of corner area in the section area. Table 2 and Figure 6 illustrate that in the sections the corner area has more contribution, the corner radii imperfections have more impact.

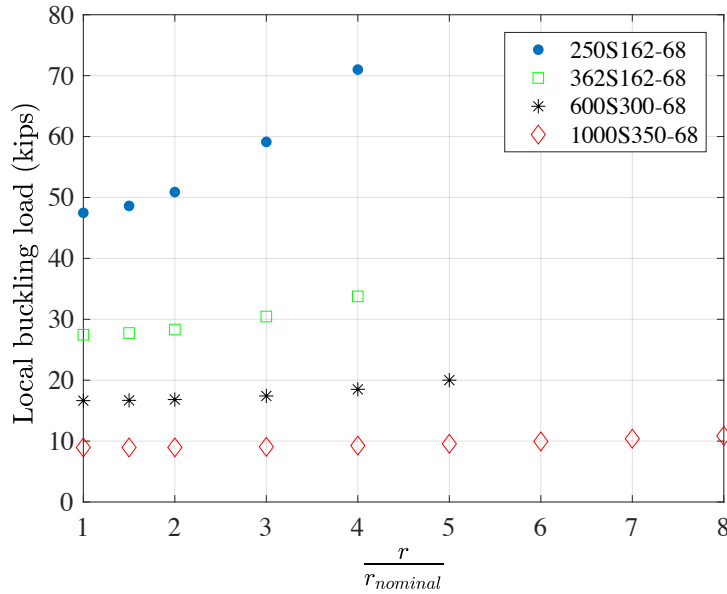


Figure 4: Local Buckling load of perfect and imperfect sections

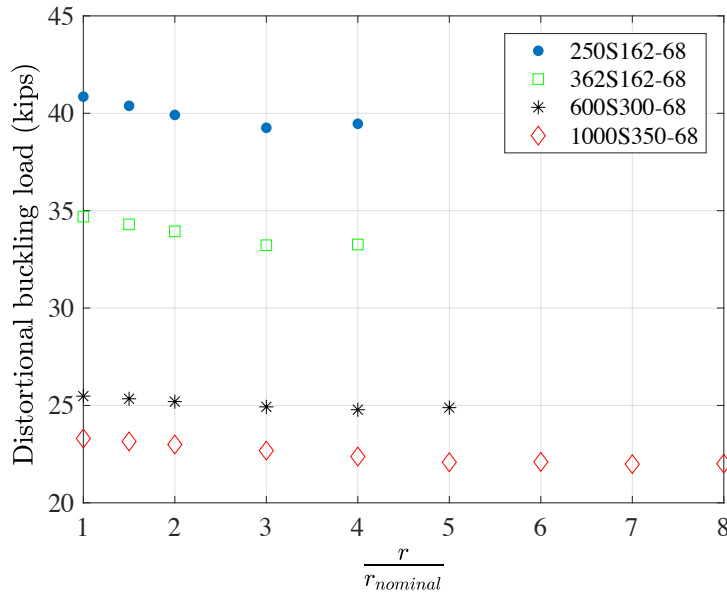


Figure 5: Distortional buckling load of perfect and imperfect sections

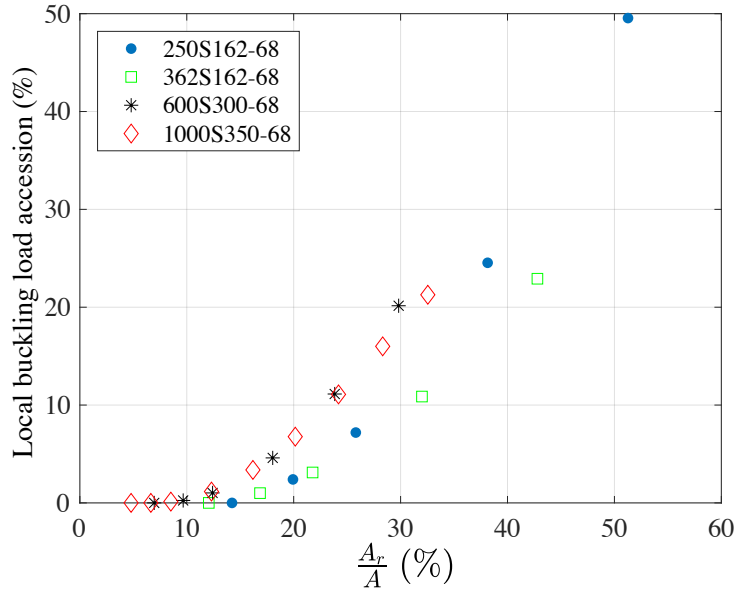


Figure 6: Impact of corner area on the local buckling load increase

The impact of corner radius imperfection is explored and as the results show, it can have an impact on the section strength especially on small sections. A photogrammetry-based tool is proposed to measure imperfect corner radii to be considered in analyses.

### 3. Photogrammetry

The pixel is considered as the smallest single component of a digital image. They are physical points creating a digital image by standing next to each other. As a result, more components can represent more detail from an object in digital images. In Figure 7.a as an example, a key and its individual pixels rendered as small squares can be seen easily. Each pixel is represented by one or more numerical values. The number of distinct colors that can be represented by a pixel depends on the number of bits per pixel (bpp). Binary images are encoded as a 2D array, which usually uses 1 bit per pixel. In this type of images, the pixel value of 0 usually means black and 1 means white. Grayscale images are also encoded as a 2D array of pixels with 8 bits per pixel, in which a single value represents the intensity of a pixel in a [0,255] range. A pixel value of 0 means black, a pixel value of 255 means white, and middle values show varying shades of gray. Color images can be represented using three same size 2D arrays indicating the amount of red (R), green (G), and Blue(B) which are known as RGB color channels (Figure 7). Each pixel is usually formed by a 24-bit number containing the amount of its RGB components. Each array element contains an 8-bit value, representing the amount of red, green, and blue at the point in a [0,255] range (Marques, 2011).

The proposed tool works with grayscale images, while the images taken by users' cell phones are usually color images; hence, the first step is transforming color images to grayscale ones. In order to help the tool to distinguish the desired object from its background in a monochrome image, it is recommended that for dark objects, the user provides a bright background and the reverse for bright objects.

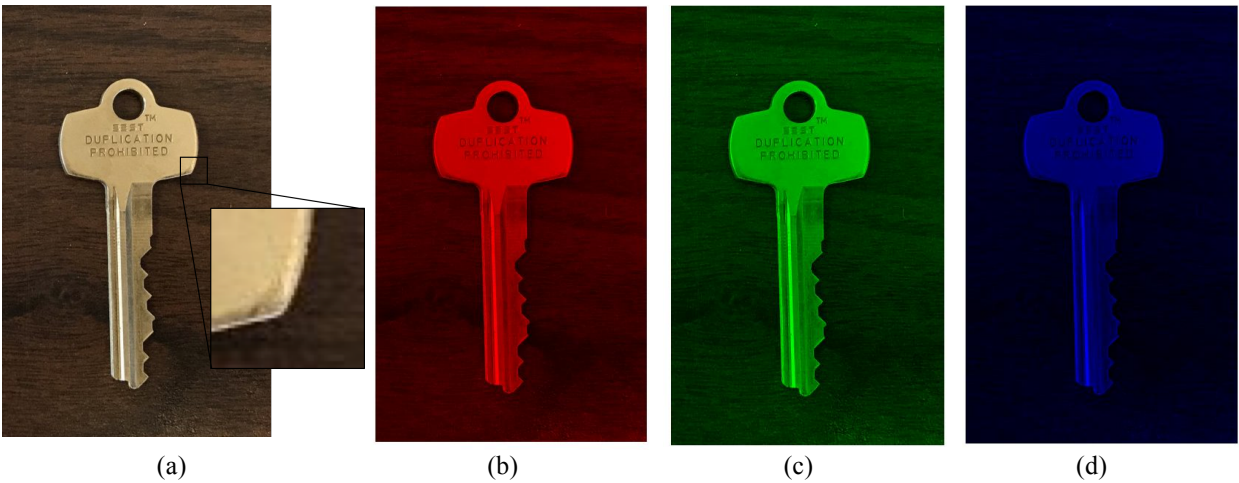


Figure 7: Digital image of a key and its pixels in addition to its RGB color channels; (a) original image of a key and its pixels; (b) red color channel; (c) green color channel; (d) blue color channel

The grayscale images made by the tool have noise the source of which is usually the shadow made by the object or is the dirt on the background. For an image with a dark object and a white background, the grayscale image made by the tool consists of an almost black object and a gray background. This gray background is caused by shadows and the background which is not completely white (pixel value of 255). Therefore, the user should define a specific pixel value that pixels with values greater than that become completely white, and pixels having smaller ones become completely black with pixel value equal to zero. In other words, the tool transforms grayscale images to binary images. As an example, in order to detect the cross-section of a hot rolled channel, because the channel is considered as a dark object, we could provide a white background; however, due to the perspective, as it can be seen in Figure 8, the image taken from the top also captures the depth of the section which is not desirable. Hence, the desired section is painted white and the section depth and the lab floor is considered as a dark background. The image is read by the tool and it transforms the image to a grayscale one. For the first try, the pixel value 140 is set for the tool and it makes pixels with pixel value less than 140 black and the rest white (Figure 8.b). As it can be seen, the parts which are brighter like the top left corner of the image are still white so the pixel value limit should be increased (Figure 8.c). There are still white pixels around the section which should be omitted. Therefore, in the last try the pixel value 175 is set for the tool and the section is detected completely with details and black background (Figure 8.d).

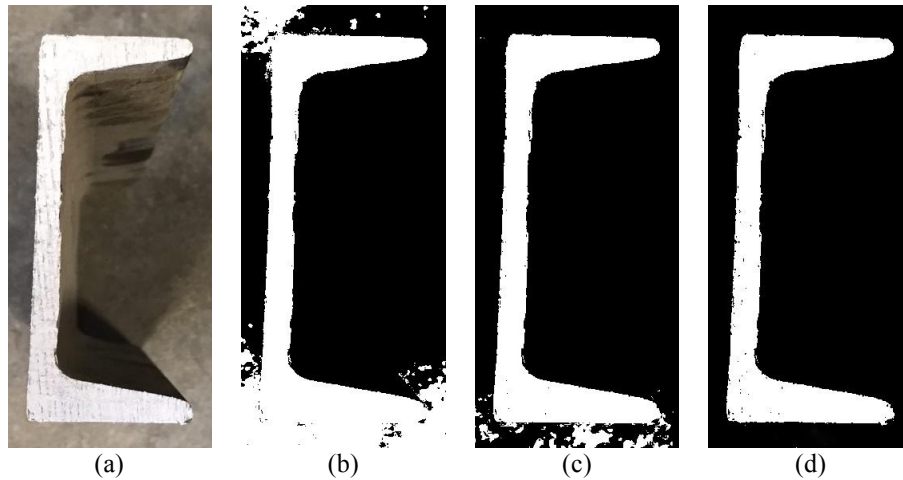


Figure 8: Section detection of a hot rolled steel channel; (a) original image; (b) the result of section detection when 140 is set for pixel value; (c) the result when 160 is set; (d) the result when 175 is set

#### 4. Measuring dimensions

The concept of measuring dimensions used in the tool is based on counting the pixels. The tool counts the pixels located in the desired direction, then by a scale, the number is converted to a unit of measurement. For example, a one-inch square is printed on a piece of paper. The tool as it is shown in Figure 9 counts the number of pixels in the X direction. Then the angle of the square with the horizon is calculated because the image may be taken with angle or the paper may be placed with an angle on the table, which means the counted number is not the pixel number of the square sides. As a result, as it can be seen in Table 3, the number of pixels located on the side of the square is measured. This concept is utilized for measuring the thickness and dimensions of the section. By this method, the user can measure the thickness of everywhere and the mean of thicknesses can be used as the input for computational methods. A square with a specified dimension can be used as a scale, which will be discussed.

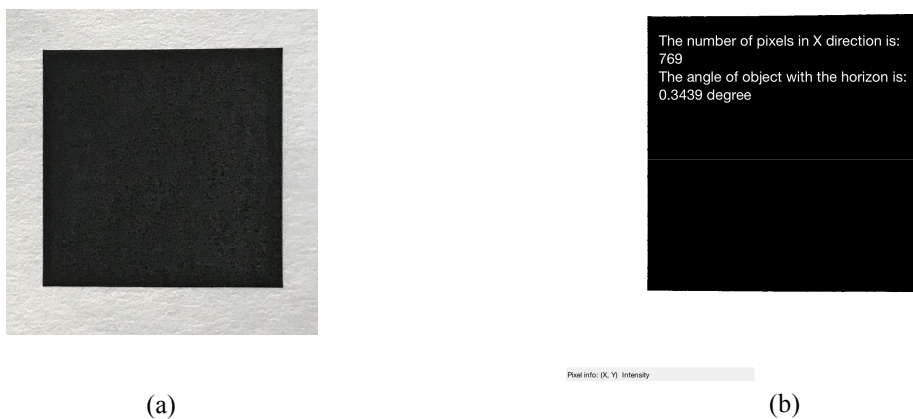


Figure 9: Counting the number of pixels for one side of a one-inch square; (a) original image; (b) the output of the tool

Table 3: Pixels in x direction for a one inch square

The number of pixels in X direction	Angle of the object with horizon (degree)	The number of pixels in the side of square	The length each pixel represents
769	0.3439	768.9861	0.0013

### 5. Measuring the corner radius

Every corner has two radii: inside and outside corner radii. To measure these radii the tool detects the inner and outer boundary of the section. The corners usually connect a web to flanges or connect a flange to the section lips. Hence, the corners are considered as a circle cut between two straight line. In fact, the aim of the tool is looking for a circle which is tangent to both of the mentioned lines. The radius of this circle would be the corner radius and the angle can be considered as an imperfection compared to the perfect section. As a result, the tool should find one point on each line where the circle is tangent to the lines. As it can be seen in Figure 10, the mentioned points are the last point (pixel) located on straight lines and the curve starts and finishes in these points. In other words, the next point or pixel has a very small distance equal to the  $\epsilon$  to the extended line. A default  $\epsilon$  is defined for the tool but the user can enter his  $\epsilon$ .

In a perfect section, their boundaries are perfectly straight; however, in real sections, the boundaries are jagged which is usually due to the cutting process. The pixels are very sensitive to this issue and in order to capture the jagged boundaries, they cannot be placed in a straight line. The user should define a segment for each leg e.g. web or flange which he is sure this segment is completely straight and does not contain any part of the corner. Then fitted lines to the inner boundary of each segment is considered as the perfectly straight boundaries. A line is fitted to the numerous pixels; hence, it is obvious that the pixels have a distance to the fitted line already, so here the  $\epsilon$  plays a significant role in finding the two pixels/points where the corner curve starts and finishes. Now, the tool has both beginning and end points of the corner, and it has two lines tangent to the user desired circle. The center of the circle is determined by finding the intersection of two lines perpendicular to the edge lines in beginning and end points; by having the center and those two points, the radius is measured.

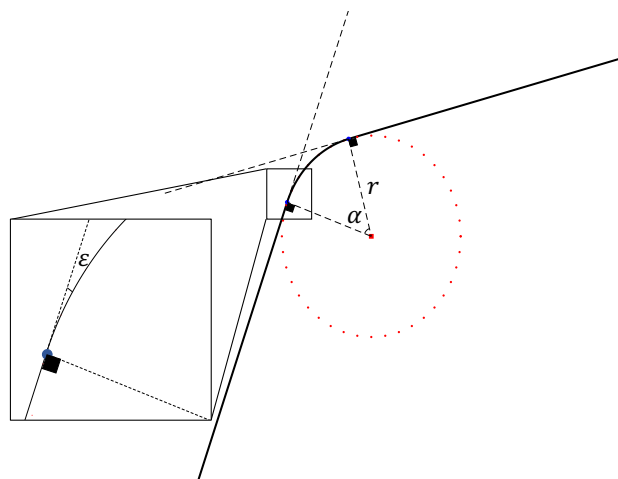


Figure 10: Methodology of calculating corner radius

## 6. Scale

As mentioned before, the tool calculations are based on the pixel and the output is the number of pixels counted. In order to utilize measurements done by the tool in computational methods such as finite strip method analysis, the outputs are needed to be converted to the measurements units. Hence, the user should provide a scale. A scale is an object which its dimensions are known for the user. This scale can be another object with known dimension like a square printed on a piece of paper or it can be a measurement done in the lab. In the first method, the scale should be placed in the same elevation as the desired object. It should be noted that the photo taken from the object and the scale should have the completely same condition to increase accuracy; as a result, it is recommended that the user only take one photo consisting of both the object and the scale, then by cropping the scale from the original photo makes two separate ones. The next step is running the software two times, One run for the object and another one for the scale. In the second method, the user should do a precise measurement in the lab. For instance, for a CFS stud, the user can measure the thickness of the section by a caliper in a certain position and do it again in the tool, then convert the tool outputs to measurement units.

## 7. Example

In order to measure the corner radius of a non-structural CFS track (362T125-18), a photo is taken from its top by a standard cell phone camera. The nominal corner radius of the section is mentioned in Table 4. In order to increase the measurement precision and decrease the perspective and angle of photography effects, a photo consists of only a corner and a part of web and flange is taken (Figure 11.a). Both the specimen and background are bright; hence, a part of the section is painted by a black marker. As shown in Figure 11.b, the marked part of the section is detected properly by the tool.

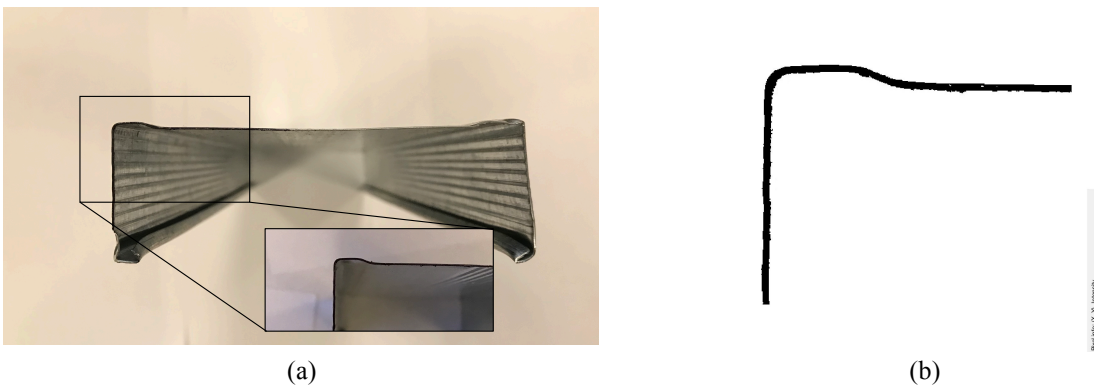


Figure 11: Detecting a CFS section by the tool; (a) original image; (b) detected image

The tool is run and it considers the detected part as its input. The start and finish points, center, corner angle, and corner radius are measured. It should be noted the corner radius is based on the pixel and it should be converted to a unit of measurement. For this purpose, the thickness of the specimen is measured by caliper which is 0.0215 inch. The thickness is measured by the tool as well. The summary of measurement is shown in Table 4. The corner radius and corner angle of the imperfect section are 2.82% and 3.50% smaller than nominal ones respectively. Two sources are likely responsible for this difference: section imperfection and the tool inaccuracy.

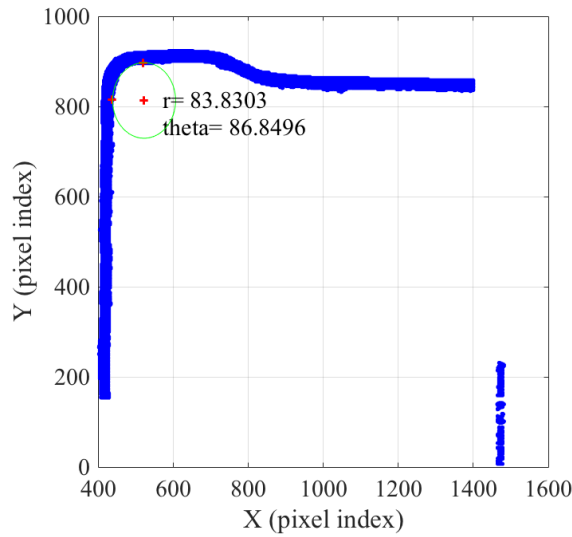


Figure 12: Corner radius and corner angle measurement done by the tool

Table 4: Summary of measurements done by the tool

Perfect section		Scale			Imperfect section		
Radius (in.)	Angle (degree)	Measured thickness (in.)	Measured thickness (pixel)	The length each pixel represents	Radius (Pixel)	Radius (in.)	Angle (degree)
0.0843	90	0.0215	22	9.8E-4	83.8303	0.0819	86.85

The section properties of both perfect and imperfect 362T125-18 are imported into the CUFSM and finite strip analysis is performed. The distortional buckling of the perfect section is 2.7782 kips. and distortional buckling of imperfect one is 2.7754 kips. The signature curves of these sections which are almost same are plotted in Figure 13. Due to the small thickness of the section,

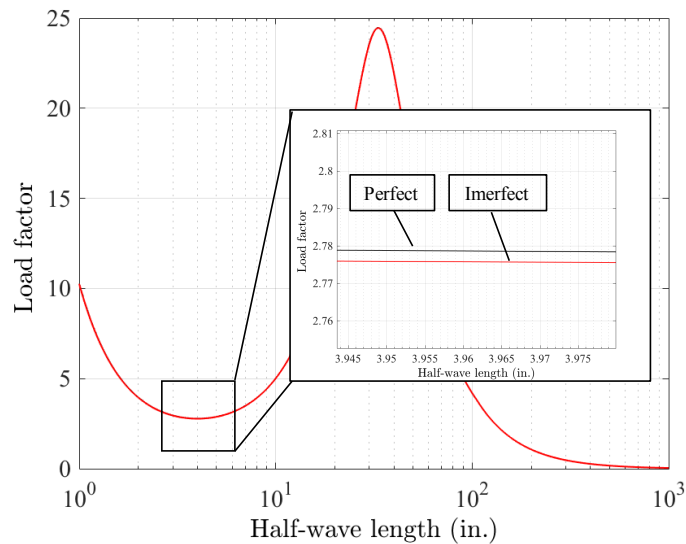


Figure 13: Signature curves of perfect and imperfect 362T125-18

the corner radius is too small, and corner area has a small contribution in the section area. Therefore, the impact of the imperfect corner radius on the specimen strength is negligible and signature curves are practically same.

## 8. Conclusion

The impact of corner radius imperfection on the stability performance of CFS sections is explored. According to the type of buckling and the section geometry, an imperfect corner radius can play a significant or insignificant role. For the examined studs, increased corner radii may have a positive impact on the local buckling load while the reverse is true for the distortional buckling load. In the sections with large webs and flanges (such as the 1000S sections considered herein), the imperfect corner radii may have less impact in comparison with small sections (such as the 250S sections). In order to measure the corner radii of the specimens, an open source and portable tool using photos taken by standard cell phones which does the measurements based on the photogrammetry is proposed. An example done for a CFS section shows this tool can be deployed for measuring imperfections and the tool output can be imported into the CUFSM for finite strip method analysis.

## Future work

To package the tool for open source download and easy distribution, the tool must be streamlined and organized for universal ease of use. The imperfection of more CFS specimens should be captured to determine the impact of corner radii on their strength. One admittedly major drawback of the tool is that it performs imperfection measurements on the cross-sections ends, which are particularly prone to geometric imperfections due to the cutting process. However, using existing full-field imperfection measurements, the authors will create an analytical adjustment parameter to transform cross-section end measurements into measurements representative of the midspan of the cross-section.

## Acknowledgments

The authors would like to gratefully thank the University of Massachusetts Amherst for their financial support and Mark Gauthier, the University of Massachusetts Amherst lab technician for his help.

## References

- Dubina, D., & Ungureanu, V. (2002). Effect of imperfections on numerical simulation of instability behaviour of cold-formed steel members. *Thin-Walled Structures*, 40(3), 239–262.
- Zeinoddini-Meimand, V. (2011). Geometric Imperfections in Cold-formed Steel Members. Ph.D. thesis. Johns Hopkins University, Baltimore, Maryland, USA.
- Moen, C. D., Igusa, T., & Schafer, B. W. (2008). Prediction of residual stresses and strains in cold-formed steel members. *Thin-Walled Structures*, 46(11), 1274–1289.
- Zeinoddini, V., & Schafer, B. W. (2010). Impact of corner radius on cold-formed steel member strength. *20th International Specialty Conference on Cold-Formed Steel Structures - Recent Research and Developments in Cold-Formed Steel Design and Construction*, 1–15.
- Schafer, B. ., & Peköz, T. (1998). Computational modeling of cold-formed steel: characterizing geometric imperfections and residual stresses. *Journal of Constructional Steel Research*, 47(3), 193–210.
- Young, B., & Rasmussen, K. J. R. (2003). Measurement techniques in the testing of thin-walled

- structural members. *Experimental Mechanics*, 43(1), 32–38.
- McAnallen, L. E., Padilla-Llano, D. A., Zhao, X., Moen, C. D., Schafer, B. W., & Eatherton, M. R. (2014). Initial geometric imperfection measurement and characterization of cold-formed steel C-section structural members with 3D non-contact measurement techniques. *Structural Stability Research Council Annual Stability Conference 2014, SSRC 2014*, 1–25.
- Zhao, X., Tootkaboni, M., & Schafer, B. W. (2017). Laser-based cross-section measurement of cold-formed steel members: Model reconstruction and application. *Thin-Walled Structures*, 120(November 2015), 70–80.
- Schafer, B. W., & Ádány, S. (2006). Buckling analysis of cold-formed steel members using CUFSM: conventional and constrained finite strip method. *18th International Specialty Conference on Cold-Formed Steel Structures*.
- Marques, O. (2011). *Practical image and video processing using MATLAB*. Hoboken, N.J.: Wiley-IEEE Press.